Journal of Materials Chemistry A

Accepted Manuscript

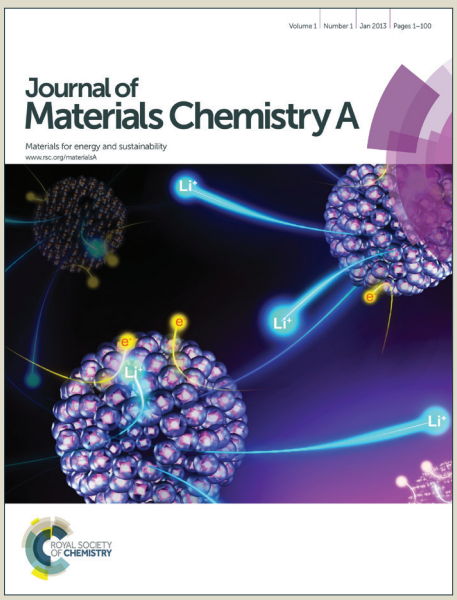

ROYAL SOCIETY OF CHEMISTRY

www.rsc.org/materialsA

Mesoporous carbon/silicon composite anodes with enhancement performance for lithium-ion batteries

Yunhua Xu, Yujie Zhu, Chunsheng Wang*

Department of Chemical and Biomolecular Engineering, University of Maryland, College Park, MD 20742, USA
* Corresponding author. Tel.: +1 301 405 0352; fax: +1 301 405 0523.
E-mail address: cswang@umd.edu (C. Wang)

Keywords: silicon, mesoporous carbon, anode, lithium-ion battery, soft template

Abstract: Silicon offers the highest theoretical capacity among all investigated anode materials for Li-ion batteries, making it a promising alternative anode to the currently-used graphite. However, Si anodes still face significant challenges for commercialization due to the poor cycling performance induced by the huge volume change (300%) during the insertion/extraction of lithium ions. In this paper, we report a mesoporous C/Si composite synthesized by organic-organic self-assembly of triblock copolymer and resorcinol–formaldehyde resin. The larger number of hydroxyl groups of RF resin directs the formation of mesostructure and coating/dispersion of Si nanoparticles through strong hydrogen bonding interaction. The mesoporous carbon matrix efficiently accommodates the volume change of nano-Si and to maintain the integrity of the nano-Si electrodes. Significantly improvement in electrochemical performance has been demonstrated in comparison with the bare Si nanoparticle anodes. In the meanwhile, the synthesis method can be easily scaled up for mass production.

Keywords: lithium ion battery, silicon anode, mesoporous carbon, block copolymer, self-assembly

1. Introduction

Lithium-ion batteries, the dominated power sources for portable electronic devices, have been recognized as the most promising technology for next generation energy storage for electric vehicles and renewable energy. However, the graphite anodes used in current commercial Li-ion batteries have a limited capacity (372 mAh/g), which restricts its application for electric vehicles. As one of the most promising alternative anodes to graphite, silicon offers a theoretical capacity of 3579 mAh/g upon full intercalation state of $Si_{15}Li_4$ at room temperature, which is ten times higher than that of graphite and, to date, is the highest capacity among all investigated anode materials.

However, Si anodes suffer from huge volume change (300%) during the insertion/extraction of lithium ions, resulting in particle pulverization, losing electric connection between the Si particles and the current collector as well as continuous growth of solid-electrolyte interface (SEI) film, thus fast capacity fading.[1,2] In addition, the low electronic conductivity of Si also lowers the power density. Extensive efforts have been made to improve the cycling stability and power density.[3-25] The most successful strategies are to use graphene,[6-9] carbon tubes,[10-15] hollow or porous carbon[16-23] to accommodate the stress/strain of Si induced by volume change and enhance the electronic conductivity. However, most C/Si composite materials are synthesized using complicate and expensive high-temperature chemical vapor deposition,[6,10-12,14.15.22] or hard template,[13,16-18,20] which limits the practical applications for mass-production.

Mesoporous carbon, possessing good conductivity, high resiliency, good mechanical strength and large porosity, is an ideal support matrix for Si nano-particles, which can efficiently alleviate the stress/strain and volume change of Si particles. Among all synthesis methods for mesoporous carbon, the most facile and cost-efficient route is organic-organic self-assembly method using

commercial precursor materials followed by carbonization process,[26-29] in which phenolic resins and triblock copolymers of poly(ethylene oxide)-b-poly(propylene oxide)-b-poly(ethylene oxide) (PEO-PPO-PEO) were used as carbon precursor and structure-directing agents, respectively. The hydrogen bonding between the hydroxyl groups of phenolic resin and the polyethylene (PEO) chains of copolymers direct the formation of mesostructures. Recently, Park et al. reported a mesoporous carbon/Si nanoparticle composite using triblock copolymer of Pluronic F127 and phenol–formaldehyde (F) polymer as the template agent and carbon precursor, respectively.[30] Si nanoparticles were well coated with carbon and uniformly distributed in the mesoporous carbon due to the hydrogen binding interaction between the large number of hydroxyl groups (–OH) of the phenol–formaldehyde resin and the oxide layer on the surface of the Si nanoparticles.

It has been shown that the density of the hydroxyl groups in the phenolic resin is a key factor to the formation of mesostructures and the surface coating of Si particles.[27,28,31] Resorcinol (R) has double number of hydroxyl groups than phenol, offering greater driving force for the self-assembly and the interaction of Si/resin. Actually, fine encapsulation/coating of Si nanoparticles with RF-resin carbon has been reported, and improved capacity and cycling stability for RF-based C/Si composites was obtained.[32-35]

Recently, we have successfully fabricated a sponge-like mesoporous C/Sn composite using RF resin as carbon precursor and triblock copolymer of poly(ethylene oxide)-b-poly(propylene oxide)-b-poly(ethylene oxide) (EO106-PO70-EO106, Pluronic F127) as the template agent, where SnO_2 nanoparticles were dispersed into the RF resin/F127 precursor matrix followed by carbonization.[36] In the mesoporous C/Sn composite, the mesoporous carbon matrix can efficiently accommodate the volume change of Sn nanoparticles, thus largely enhancing the cycling stability. In this study, this strategy was used for Si anodes. The plenty of hydroxyl

groups on the surface of Si and RF resin give to a strong interaction between them via hydrogen bonding, which ensures a fine coating and dispersion of Si nanoparticles within mesoporous carbon matrix. Significant improvement in electrochemical performance was demonstrated.

2. Experimental

2.1 Synthesis of mesoporous C/Si nanoparticle composite

The synthesis of mesoporous C/Si composite materials consisted of three steps: preparation of precursor solution and dispersion of Si nanoparticle, in-situ polymerization, and carbonization. All materials were purchased from Sigma-Aldrich and were used without further purification. 0.3 g Si nanoparticles (<100 nm) were dispersed into 20 ml *N,N*-dimethylformamide (DMF) through ultrasonication. In the meanwhile, the precursor solution was prepared by dissolving 0.165 g resorcinol (R), 0.1 g triblock copolymer Pluronic F127 and 0.03 g 37% HCl aqueous solution in 5 ml DMF, where the triblock copolymer and HCl functioned as soft-template and catalyst, respectively. When the solution turned clear, 0.195 g 37% formaldehyde (F) aqueous solution was added. After 30 min vigorous stirring, the solution was stirred for another 30 min at 80 ºC to prepolymerize precursors of resorcinol and formaldehyde. Then the resulting solution was added into the Si dispersion and underwent ultrasonic treatment. The mixture was dried while stirring at 100 °C overnight and further cured in an oven at 100°C for 24 h. Finally, the polymer/nano-Si composite was carbonized at 400 °C for 3 h and then 700 °C for additional 3 h in flowing argon with heating ramp of 2 °C/min. Pure mesoporous carbon without Si was also synthesized using the same procedure described above.

2.2 Material Characterizations

Scanning electron microscopy (SEM) and transmission electron microscopy (TEM) images were taken by Hitachi SU-70 analytical ultra-high resolution SEM (Japan) and JEOL (Japan)

2100F field emission TEM, respectively. Thermogravimetric analysis (TGA) was carried out using thermogravimetric analyzer (TA Instruments, USA) with a heating rate of 10 °C/min in air. BET specific surface area and pore size and volume were analyzed using N_2 absorption on TriStar 3020 (Micromeritics Instrument Corp., USA).

2.3 Electrochemical Measurements

The mesoporous C/Si composite was mixed with carbon black and sodium carboxymethyl cellulose (CMC) binder to form a slurry at the weight ratio of 70:15:15. The mesoporous C/Si electrode with active material loading of ~1 mg/cm^2 was prepared by casting the slurry onto copper foil using a doctor blade and dried in a vacuum oven at 100 °C overnight. Coin cells were assembled with lithium foil as counter electrode, 1M $LiPF_6$ in a mixture of fluoroethylene carbonate/dimethyl carbonate (FEC/DMC, 1:1 by volume) as the electrolyte, and Celgard®3501 (Celgard, LLC Corp., USA) as the separator. Cells with bare nano-Si electrodes were also fabricated using the same procedure. Electrochemical performance was tested using Arbin battery test station (BT2000, Arbin Instruments, USA) at the voltage range of 0.02 – 1.5 V. Capacity was calculated on the basis of Si mass. Impedance data were recorded using Solatron 1260/1287 Electrochemical Interface (Solartron Metrology, UK).

3. Results and Discussion

The mesoporous carbon was synthesized using resorcinol-formaldehyde (RF) polymer as carbon source, and triblock copolymer of Pluronic F127 as sacrificial template to form pores.[26-29] Fig. 1 illustrated the formation of the self-assembly nanostructure of RF-resin/F128 and the coating process of Si nanoparticles. The RF resin contains a large amount of hydroxyl groups, which allow them to form a hydrogen bond with the hydrophilic blocks of the triblock copolymer F127 or the hydroxyl groups on the surface of Si nanoparticles. Thus a thin layer of

RF resin was coated on the surface of Si nanoparticles. In the meantime, the copolymer surfactant of Pluronic F127 and RF resin would also be drove to form mesophase structure matrix under the self-assembly process. It should be noted that the different surface energy of the Si surface and the RF resin may affect the self-assembly behavior, especially the area close to the surface of Si nanoparticles.[37] The triblock copolymer decomposes in the subsequent carbonization to create pores, and the RF polymer framework was carbonized to form carbon walls or coating carbon of Si nanoparticles.

Fig. 2a – d shows the SEM image of the pure mesoporous carbon and the mesoporous carbon/Si composite. Well-defined and uniform pore structure with a pore size of ~10 nm and ~ 5 nm carbon walls was observed in the mesoporous carbon (MC) (Fig. 2a). In contrast to the uniform pores and highly ordered structure of pure carbon, the mesoporous structure was clearly observed in the C/Si composite but with random geometric pore shape and order (Fig. 2c and d). This is believed to be associated with the difference in surface energy between the Si nanoparticles and RF resin. In Fig. 2c, the peeling-off of Si particles (marked with red circles) show bright cycles on edge and a lower clarity than the surrounding area. The high resolution TEM image (Fig. 2f) further reveals that a thin layer of carbon with thickness of ~5 nm is uniformly coated on the surface of Si nanoparticles as marked with red dashed lines in Fig. 2f, which strongly revealed that a thin layer of carbon was coated on the surface of Si nanoparticles. These confirm the strong interaction between RF resin and Si surface. The low-magnification SEM (Fig. 2b) and low-resolution TEM images (Fig. 2e) of the porous C/Si composite show a uniform distribution of Si nanoparticles in the carbon matrix.

The very thin carbon walls form a continuous carbon network to provide an efficient electron transportation pathway, while the continuous pores function as ion transport channels and strain

absorber. In combination of the resiliency of carbon walls with the large number of mesopores between the carbon walls in the carbon matrix, the mesoporous carbon matrix will provide flexible mechanical support for the nano-Si during lithiation/delithiation.

The mesoporous structure in the mesoporous C/Si composite was further characterized by N_2 adsorption measurement. Fig. 3a depicts the adsorption isotherm. The Brunauer – Emmett – Teller (BET) specific surface area and pore volume of the MC/Si composite are 210 m^2/g and 0.29 cm^3/g, respectively. The large pore volume of the carbon matrix could alleviate stain/stress induced by the large volume change of nano-Si, and the large specific surface area improves the electrochemical reaction kinetics. The pore size distribution from Barrett – Joyner – Halenda (BJH) measurement shows that the average pore size is 9.8 nm (Fig. 3b), which is in good agreement with that by SEM and TEM images in Fig. 2.

The carbon content in the mesoporous C/Si composite was determined using thermogravimetric analysis (TGA) analysis in air. Fig. 4 shows the thermogravimetric curve of the mesoporous C/Si composite. No weight loss was observed below 450 °C, indicating that the mesoporous C/Si composite is thermally stable in ambient air. A sharp mass loss occurred between 450 and 580 °C due to carbon decomposition. The slight increase in the high temperature range is attributed to Si oxidation. The Si content in the composite is calculated at 76% by weight.

The electrochemical performance of the mesoporous C/Si composite was investigated using coin cells. Fig. 5a shows the charge/discharge profiles of the mesoporous C/Si composite in the initial 5 cycles. In the first lithiation, the potential gradually decrease with content of Li and then followed by a long flat discharge plateau at ~ 0.08 V. The slope potential decrease of the MC/Si anodes in the high potential area (Fig. 5a) is mainly attributed to the lithiation of the mesoporoue

carbon (Fig. 4b), while the flat discharge plateau at ~ 0.08 V is a typical lithiation behavior of crystal Si anodes.[3-5] The small plateaus at 0.8 V in the first discharge of C/Si anodes (Fig. 5a) that disappeared in the following cycles is attributed to the formation of SEI films due to the decomposition of the electrolytes on porous C as shown in Fig. 5b. The formation of SEI film leads to irreversible capacity, consuming Li ions that are a limited resource usually stored in and carried by the cathode upon cell assembly, thus lowering the Coulombic efficiency. The mesoporous C/Si composites deliver charge capacities of 1461 with a Coulombic efficiency of 54%. The high irreversible capacity in the first cycle is mainly due to the large surface area of the mesoporous C/Si composite that large amount of SEI film was formed on the surface of mesoporous carbon (Fig. 5b). This is confirmed by the ultralow Coulombic efficiency of 34% for the pure mesoporous carbon anodes (Fig. 5c). After two cycles, the Coulombic efficiency of the mesoporous C/Si composite jumped to higher than 97%, indicating a good reversibility of the mesoporous C/Si composite. The charge process shows a slope plateau between 0.2 and 0.7 V, a typical feature of delithation reaction of amorphous Li_xSi. In the following cycles, the typical electrochemical behavior of amorphous Si anodes were observed with discharge/charge slopes at 0.2/0.5 V, respectively. The phase transition from crystalline to amorphous after the first cycle is a typical behavior for Si anodes.[3-5]

To examine the stability of the mesoporous C/Si composite, mesoporous C/Si anodes were cycled between 0.02–1.5 V at a current density of 500 mA/g. For comparison, the electrochemical performance of bare nano-Si and mesoporous carbon were also tested in the same conditions. Fig. 5c shows the cycling stabilities of mesoporous carbon, bare nano-Si, and mesoporous C/Si composites. Compared with the bare Si nanoparticles, the cycling performance of mesoporous C/Si composite is significantly improved. The mesoporous C/Si composite

delivered a reversible capacity of 1410 mAh/g in the first cycle, and retained a capacity of 1018 mAh/g after 100 charge/discharge cycles, which is still three times higher than graphite. The cycling performance of the porous C/Si composite is much better than that of previous porous C/Si composites synthesized using phenolic resol precursor (700 mAh/g after 50 cycles)[30] and nano $CaCO_3$ template (594 mAh/g after 50 cycles).[38] In contrast, although bare Si nanoparticles show a little higher reversible capacity of 1644 mAh/g in the first cycle, only 59 mAh/g retained after 100 cycles, revealing a fast capacity fading. Mesoporous carbon shows a high cycling stability, but the capacity of 220 mAh/g is too low. The role of pure mesoporous carbon is to provide an electrochemically stable mechanical support. The capacity and stability of the RF porous C/Si anodes are superior to those RF coated Si anodes[32-35] and phenol-formaldehyde-based porous C/Si anodes.[30] There is no doubt that the enhancement in cycling performance is attributed to the incorporation of the mesoporous carbon matrix made of RF resin.

The rate performance of mesoporous C/Si composite and the bare nano-Si anodes was compared in Fig. 5d. In addition to the poor cycling stability, the bare nano-Si anodes also suffer fast capacity roll-off as the current increased, and fail to deliver any capacity when the current increased to 1000 mA/g. On the contrary, a capacity of ~1220 mAh/g was retained at 1000 mA/g for the mesoporous C/Si composite. Even at a very high current of 10 A/g, the capacity retention of ~180 mAh/g was achieved for mesoporous C/Si anodes. The improved rate capability of the mesoporous C/Si composite is attributed to the large surface area of the mesoporous structure and conductive carbon network.

The electrochemical reaction kinetics of the mesoporous C/Si composite and bare nano-Si anodes was compared using electrochemical impedance spectroscopy (EIS) with a voltage amplitude of 10 mV in the frequency range of 10 M Hz – 0.01 Hz. Fig. 6 shows the Nyquist

plots of the fresh mesoporous C/Si and bare Si anodes. The impedance spectra consist of one depressed semicircle at high frequencies and a slopping line at low frequencies. The depressed semicircle at high frequencies is associated with two overlapped interface impedances (i.e. SEI and charge transfer), and the low-frequency line corresponds to lithium ion diffusion. It is clearly seen that the mesoporous C/Si composite experienced much lower interface impedance than those bare nano-Si anodes, indicating a lower reaction resistance for the mesoporous C/Si composite, and thus better rate capability.

The enhancement in cycling stability and rate capability of the mesoporous C/Si composite is attributed to the merits of the mesoporous carbon matrix, including: 1) the large pore volume offers void space to accommodate the volume change; 2) the thin resilient carbon walls and coating layer on Si surface provide a mechanical support to enable good electric contact between Si nanoparticles and carbon matrix; 3) the large specific surface area and continues pore channels ensure a fast charge transfer and ion transport.

4. Conclusions

Mesoporous C/Si composite was successfully synthesized by in-situ polymerization and carbonization. Si nanoparticles were uniformly dispersed in the well-defined mesoporous carbon matrix, which offers void space and mechanical support to accommodate large volume changes and the stress induced by nano-Si. In comparison with the bare Si nanoparticles and other C-coated Si anodes, significantly improved electrochemical performance was obtained for the mesoporous C/Si composite anodes. After 100 charge/discharge cycles, the mesoporous C/Si composite anodes retained a capacity of 1018 mAh/g, which is much higher than that of bare nano-Si anodes (59 mAh/g). Better rate capability was also demonstrated for the mesoporous

C/Si composite anodes. In the meanwhile, the synthesis method is facile and simple and easily scaled up, making it attractive to mass manufacture for large-scale application.

Acknowledgement

The authors gratefully acknowledge the support of the Army Research Office under Contract W911NF1110231.

References

1 U. Kasavajjula, C. S. Wang and A. J. Appleby, *J. Power Sources*, 2007, **163**, 1003.

2 H. Wu and Y. Cui, Nano Today, 20122, **7**, 414.

3 C. Chan, H. Peng, G. Liu, K. Mcilwrath, X. F. Zhang, R. A. Huggins and Y. Cui, *Nat. Nanotechnol.*, 2008, **3**, 31.

4 H. Wu, G. Chan, J. W. Choi, I. Ryu, Y. Yao, M. T. McDowell, S. W. Lee, A. Jackson, Y. Yang, L. Hu and Y. Cui, *Nat. Nanotechnol.*, 2012, **7**, 310.

5 I. Kovalenko, B. Zdyrko, A. Magasinski, B. Hertzberg, Z. Milicev, R. Burtovyy, I. Luzinov and G. Yushin, *Science*, 2011, **334**, 75.

6 K. Evanoff, A. Magasinski, J. Yang and G. Yushin, *Adv. Energy Mater.*, 2011, **1**, 495.

7 Y. Wen, Y. J. Zhu, A. Langrock, A. Manivannan, S. H. Ehrman and C. S. Wang, *Small*, 2013, **9**, 2810.

8 X. Zhou, Y.-X. Yin, L.-J. Wan and Y.-G. Guo, *Adv. Energy Mater.*, 2012, **2**, 1086.

9 J. Ji, H. Ji, L. L. Zhang, X. Zhao, X. Bai, X. Fan, F. Zhang and R. S. Ruoff, *Adv. Mater.*, 2013, **25**, 4673.

10 A. Gohier, B. Laïk, K.-H. Kim, J.-L. Maurice, J.-P. Pereira-Ramos, C. S. Cojocaru and P. T. Van, *Adv. Mater.*, 2012, **24**, 2592.

11 W. Wang and P. N. Kumta, *ACS Nano*, 2010, **4**, 2233.

12 L. Hu, H. Wu, Y. Gao, A. Cao, H. Li, J. Mcdough, X. Xie, M. Zhou and Y. Cui, *Adv. Energy Mater.*, 2011, **1**, 523.

13 M.-H. Park, M. G. Kim, J. Joo, K. Kim, J. Kim, S. Ahn, Y. Cui and J. Cho, *Nano Lett.*, 2009, **9**, 3844.

14 B. Hertzberg, A. Alexeev and G. Yushin, *J. Am. Chem. Soc.*, 2010, **132**, 8548.

15 B. Wang, X. Li, X. Zhang, B. Luo, Y. Zhang and L. Zhi, *Adv. Mater.*, 2013, **25**, 3560.

16 N. Liu, H. Wu, M. T. McDowell, Y. Yao, C. Wang and Y. Cui. *Nano Lett.*, 2012, **12**, 3315.

17 H. Wu, G. Zheng, N. Liu, T. J. Carney, Y. Yang and Y. Cui, *Nano Lett.*, 2012, **12**, 904.

18 D. S. Jung, T. H. Hwang, S. B. Park and J. W. Choi, *Nano Lett.*, 2013, **13**, 2092.

19 Y.-S. Hu, P. Adelhelm and B. M. Smarsly, J. Maier, *ChemSusChem*, 2010, **3**, 231.

20 H. Kim, B. Han, J. Choo and J. Cho, *Angew. Chem. Int. Ed.*, 2008, **47**, 10151.

21 R. Yi, F. Dai, M. L. Gordin, S. Chen and D. Wang, *Adv. Energy Mater.*, 2013, **3**, 295.

22 A. Magasinski, P. Dixon, B. Hertzberg, A. Kvit, J. Ayala and G. Yushin, *Nat. Mater.*, 2010, **9**, 353.

23 T. H. Hwang, Y. M. Lee, B.-S. Kong, J.-S. Seo and J. W. Choi, *Nano Lett.*, 2012, **12**, 802.

24 S. H. Ng, J. Wang, D. Wexler, K. Konstantinov, Z.-P. Guo and H.-K. Liu, *Angew. Chem. Int. Ed.*, 2006, **45**, 6896.

25 J. Deng, H. Ji, C. Yan, J. Zhang, W. Si, S. Baunack, S. Oswald, Y. Mei and O. G. Schmidt. *Angew. Chem. Int. Ed.*, 2013, **52**, 2326.

26 Y. Meng, D. Gu, F. Zhang, Y. Shi, H. Yang, Z. Li, C. Yu, B. Tu and D. Y. Zhao, *Angew. Chem. Int. Ed.*, 2005, **44**, 7053.

27 Y. Meng, D. Gu, F. Zhang, Y. Shi, L. Cheng, D. Feng, Z. Wu, Z. Chen, Y. Wan, A. Stein and D. Y. Zhao, *Chem. Mater.*, 2006, **18**, 4447.

28 C. Liang and S. Dai, *J. Am. Chem. Soc.*, 2006, **128**, 5316.

29 S. Tanaka, N. Nishiyama, Y. Egashira, K. Ueyama and Chem. Commun., 2005, 2125.

30 J. Park, G.-P. Kim, I. Nam, S. Park and J. Yi, *Nanotechnol.*, 2013, **24**, 025602.

31 D. Zhao, Q. Huo, J. Feng, B. F. Chmelka and G. D. Stucky, *J. Am. Chem. Soc.*, 1998, **120**, 6024.

32 J.-K. Lee, M. C. Kung, L. Trahey, M. N. Missaghi and H. H. Kung, *Chem. Mater.*, 2009, **21**, 6.

33 G. X. Wang, J. H. Ahn, J. Yao, S. Bewlay and H. K. Liu, *Electrochem. Commun.*, 2004, **6**, 689.

34 Y. S. Jung, K. T. Lee and S. M. Oh, *Electrochim. Acta*, 2007, **52**, 7061.

35 T. Hasegawa, S. R. Mukai, Y. Shirato and H. Tamon, *Carbon*, 2004, **42**, 2573.

36 Y. H. Xu, J. C. Guo and C. S. Wang, *J. Mater. Chem.*, 2012, **22**, 9562.

37 K. Wang, W. Zhang, R. Phelan, M. A. Morris and J. D. Holmes, *J. Am. Chem. Soc.*, 2007, **129**, 13388.

38 X. Shen, D. Mu, S. Chen, B. Xu, B. Wu and F. Wu, Si/mesoporous carbon composite as an anode material for lithium ion batteries, *J. Alloy. Compoun.*, 2013, **552**, 60.

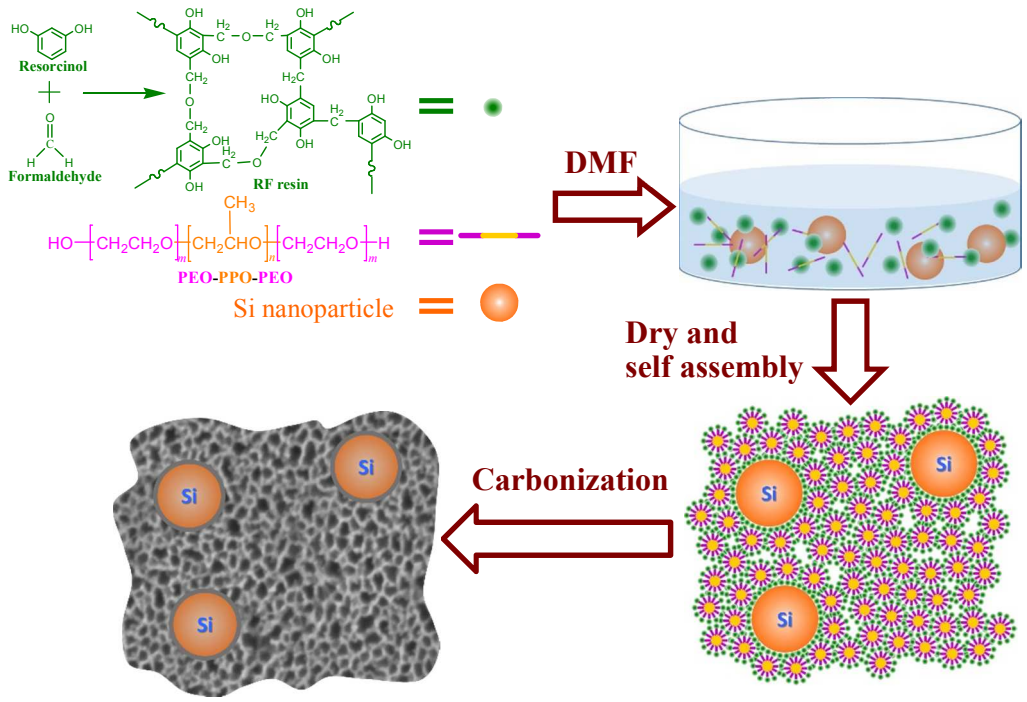

Fig. 1 Schematic illustration of the synthesis of the mesoporous C/Si composite.

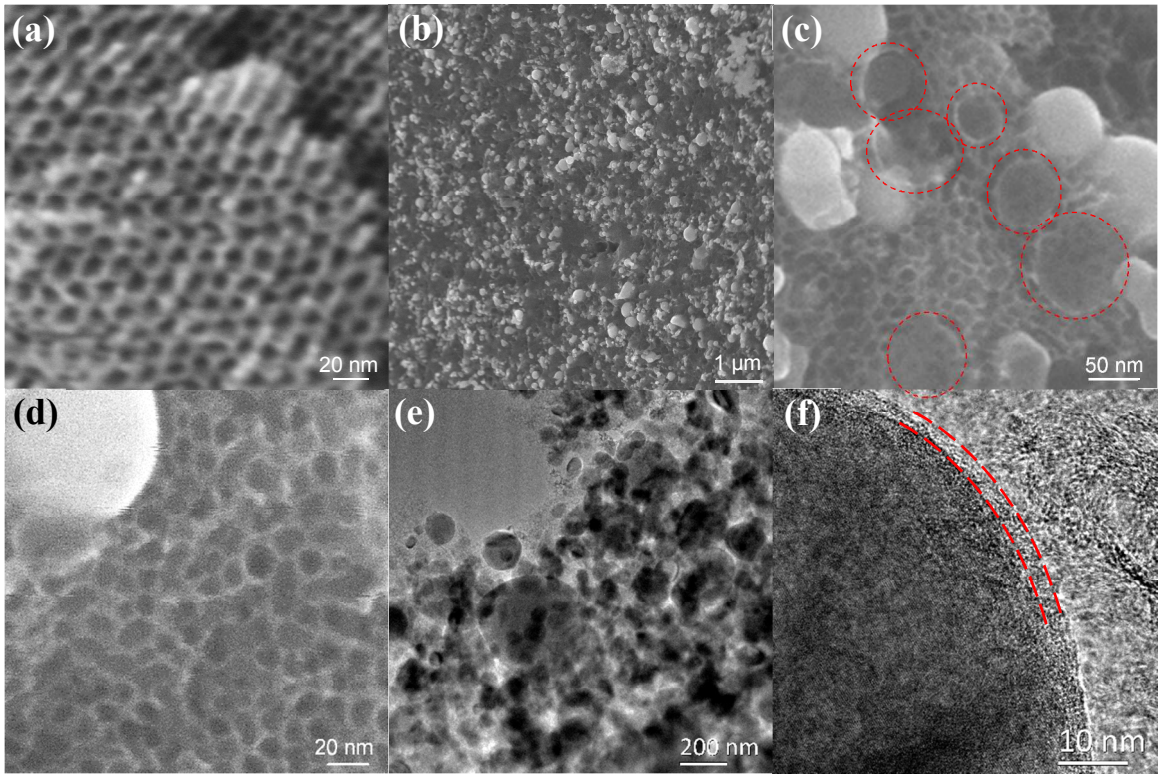

Fig. 2 SEM images of (a) the pure mesoporous carbon and (b-d) the mesoporous C/Si composites and (e, f) TEM images of the mesoporous C/Si composites.

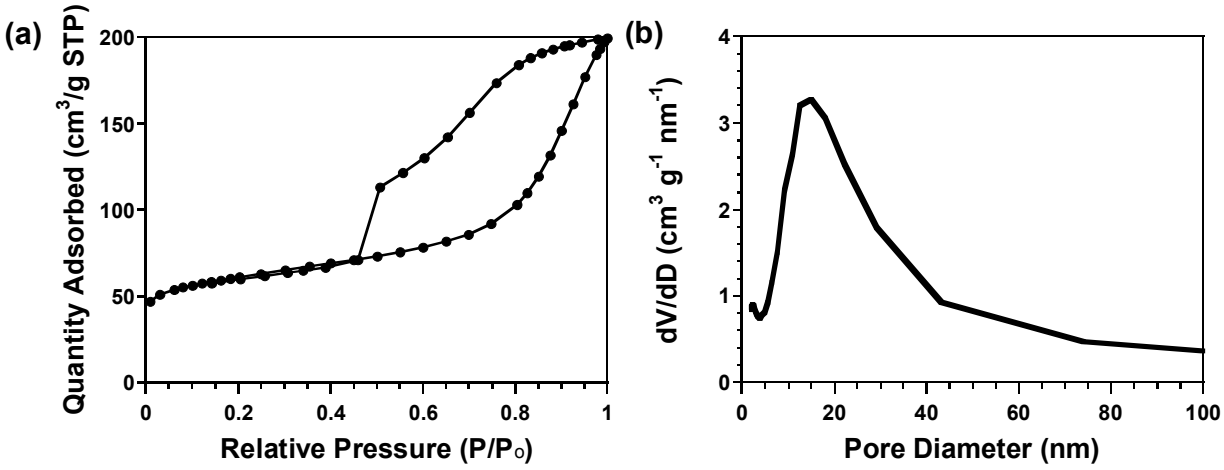

Fig. 3 (a) N_2 adsorption/desorption isotherm and (b) pore size distribution of the mesoporous C/Si composites.

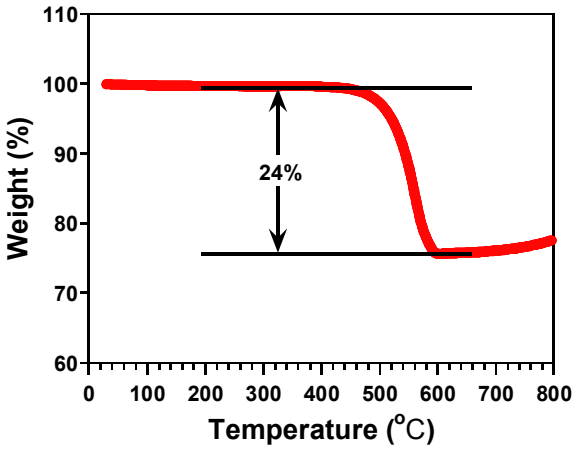

Fig. 4 Thermogravimetric (TGA) curve of the mesoporous C/Si composites in air.

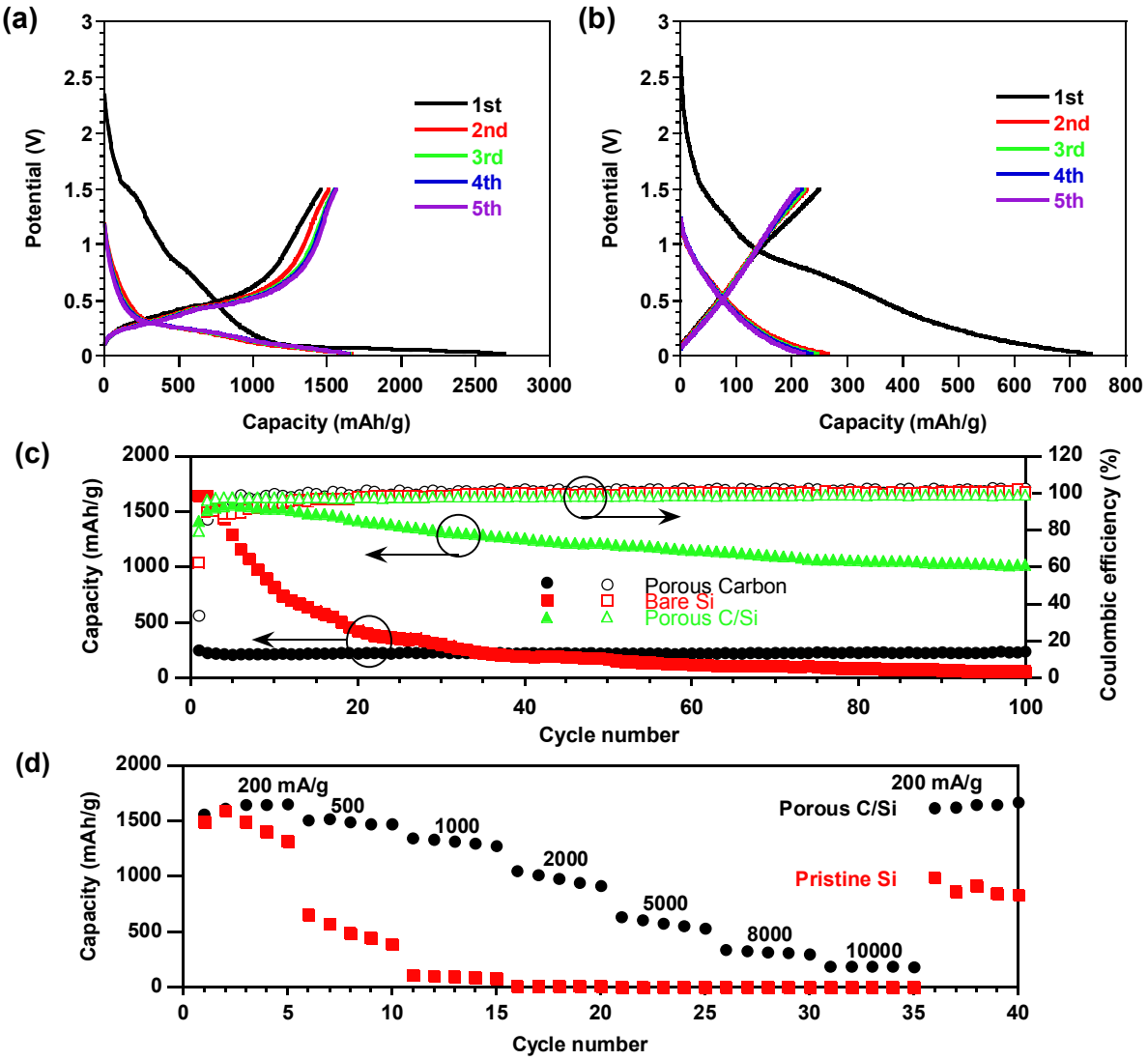

Fig. 5 Charge/discharge profiles in the first five cycles of (a) the mesoporous C/Si composites and (b) pure mesoporous carbon. (c) cycling performance, and (d) rate capability of the mesoporous C/Si composite, bare Si and mesoporous carbon anodes.

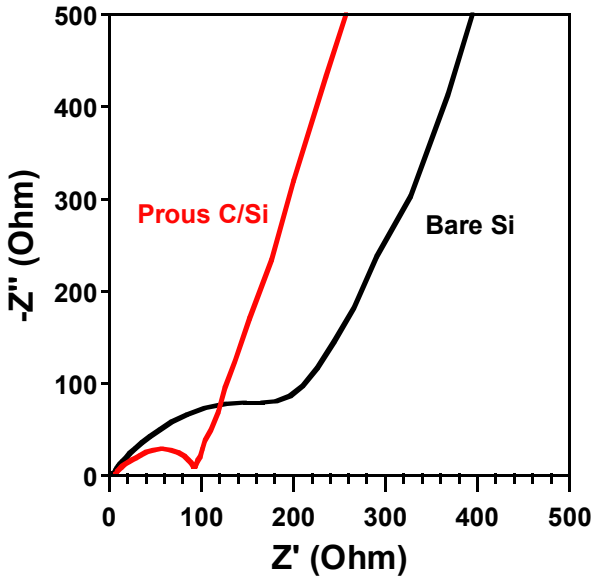

Fig. 6 Nyquist plot of the fresh mesoporous C/Si composite and bare Si anodes.

Graphical abstract

A mesoporous C/Si composite was synthesized using an in situ polymerization method via a scalable organic-organic self-assembly process. Significantly improved in cycling stability and rate capability were demonstrated for mesoporous C/Si composite.